Theoretical and numerical analysis of counter-flow parallel convective exchangers considering axial diffusion

Jules Dichamp, Frédéric de Gournay, Franck Plouraboué

Theoretical and numerical analysis of counter-flow parallel convective exchangers considering axial diffusion

J. Dichamp [a], F. De Gournay [b], F. Plouraboué [a,*]

[a] Institut de Mécanique des Fluides de Toulouse, UMR CNRS-INPT/UPS No. 5502, France
[b] Institut de Mathématiques de Toulouse, CNRS and Université Paul Sabatier, Toulouse, France

Keywords:
Generalized Graetz decomposition
Convective exchangers
Heat and mass transfer
Micro-exchangers
Compact heat exchangers

A B S T R A C T

We perform a systematic analysis of heat transfer in a counter-current three dimensional convective exchanger, when the inlet/outlet influence is fully taken into account. The analysis, carried out for constant fluid properties, considers the various influences of the fluid/solid conductivity, the imposed convection, inlet/outlet far-field conditions, and lateral boundary conditions. Using a generalized Graetz mode decomposition which permits to consider, both transverse and longitudinal diffusion influence in the exchanger as well as in the inlets/outlets, we put forward several salient generic features of convection/conduction heat transfer.

In all cases we found an optimal Péclet number for the cold or hot effectiveness. Even if, as expected, the larger the Péclet the larger the Nusselt number, high transfer performances are found to be poorly efficient and/or to necessitate non-compact elongated exchangers. Performance degradation arising at high Péclet number are found to be related to "convective leaks" taking place within outlets. A fully developed regime occurs at large Péclet and/or for long exchangers, which is fully determined by the first eigenvalue of the generalized Graetz mode decomposition, which is an extension of classical Graetz analysis. Numerical results are found consistent with a generalized linear relation between effectiveness and the number of heat transfer units asymptotically established in the convection dominated regime. This study opens new perspectives for micro-heat exchangers where moderate convection provides the best effectiveness and compactness. This contribution is also useful for giving reference solutions to counter-flow exchangers with realistic inlet/outlet boundary conditions.

1. Introduction

Conjugate counter-flow heat-exchangers are widely used in thermal and building energy, chemistry, and many other industrial applications [30]. Albeit such exchangers are of low technological content, they support important energetic functions so that proposing new tools to address their optimal use is an important technological issue. In those applied contexts, most of the exchangers are designed with the help of lumped methods, such as the traditional Log Mean Temperature Difference (LMTD) method, compartmental or transverse average approximations, in order to predict and elaborate dedicated look-up tables and graphs for each precise configuration [30,1].

At a more fundamental level, much progress have also been made in the understanding of simple geometry exchangers, e.g. parallel or axi-symmetrical configurations (e.g. [23,18,19,21,22,38,40,39,41,35,36,28] to cite only a few) during the last four decades from studying conjugated Graetz problems. In this specific context, for constant fluids properties, the convection–diffusion problem is linear and amenable to a close solution based on eigenfunction expansions. In counter-flow configurations, these solutions involve sets of real, positive and negative, eigenvalues associated with exponential longitudinal decay, upstream and downstream. Many features of those solutions can be generalized to complex fluids (e.g [29,9]).

More recently, new mathematical analysis have shown that the concept of generalized Graetz modes can be resolved when simultaneously fully taking into account longitudinal conduction and for any general tubular exchanger configuration [26,7,25]. This new framework shows that, indeed, all temperature profiles (except for the very special case of balanced, adiabatic counter-current exchanger) are varying exponentially in the longitudinal direction, in tubular exchangers. This mathematical result is indeed consistent with the LMTD method. In fact, generalized

* Corresponding author.
E-mail addresses: jules.dichamp@imft.fr (J. Dichamp), frederic.de-gournay@insa-toulouse.fr (F. De Gournay), franck.plouraboue@imft.fr (F. Plouraboué).

http://dx.doi.org/10.1016/j.ijheatmasstransfer.2016.09.019

Nomenclature

$Bi \equiv \frac{hR}{k_S}$	Biot number
$\mathcal{C}_C^E$	cold base circle in exchanger
$\mathcal{C}_H^E$	hot base circle in exchanger
C^E	external exchanger cylindrical frontier
C_C^E	cold cylinder in exchanger
C_H^E	hot cylinder in exchanger
C_{TI}^C	input cold tube
C_{TI}^H	input hot tube
C_{T0}^C	output cold tube
C_{T0}^H	output hot tube
D_0^C	cold tube disk at $z = 0$
D_0^H	hot tube disk at $z = 0$
D^C	cold tube disk
D^H	hot tube disk
D_L^C	cold tube disk at $z = L$
D_L^H	hot tube disk at $z = L$
$\epsilon_C \equiv \frac{T_C^{-\infty} - T_C^{+\infty}}{T_H^{-\infty} - T_C^{+\infty}}$	cold effectiveness
$\epsilon_H \equiv \frac{T_H^{-\infty} - T_H^{+\infty}}{T_H^{-\infty} - T_C^{+\infty}}$	hot effectiveness
Gr	Graetz number $Gr \equiv Pe/L^\star$
h	convective heat transfer coefficient (Robin/Fourier parameter)
k^F	fluid thermal conductivity
k^S	solid thermal conductivity
L	exchanger length
$L^\star = L/R$	dimensionless exchanger length
$Nu_{H,C}$	Nusselt number in hot/cold tube
$Nu_{H,C}^{loc}$	local Nusselt number in hot/cold tube
$Ntu_H \equiv Nu_H/Gr \equiv Nu_H L^\star/Pe$	number of heat transfer units
$Pe \equiv \frac{\rho c V(2R)}{k^F}$	Péclet number (balanced configuration)
Pe_C	Péclet number in cold tube
Pe_H	Péclet number in hot tube
Pe^o	optimal Péclet number
$Q_{H,C}$	flux in hot or cold tubes
$Q_{H,C}^\star$	dimensionless flux in hot or cold tubes
$Q^\star$	total dimensionless flux
R	tube radius
R_E	exchanger radius
T	temperature field
T_a	reference temperature in the air
$T_C^{-\infty}$	temperature at exchanger input in cold tube
$T_C^{+\infty}$	temperature at exchanger output in cold tube
$T_H^{-\infty}$	temperature at exchanger input in hot tube
$T_H^{+\infty}$	temperature at exchanger output in hot tube
T_w	constant wall temperature

Graetz modes analysis provides a solid theoretical foundation, as well as a clear framework for this known empirical method to be sound. It turns out that the generalized Graetz eigenfunction expansions is also useful to compute complex exchangers properties [25,24] since they permit to map a 3D problem into a 2D one (in the transverse direction). Furthermore, it is important to take into account longitudinal conduction in regions where convective effects are not dominant. Indeed, longitudinal diffusion effects were found significant for Péclet numbers as large as 100 in tubes [33,17]. But this is even more crucial inside the solid domain of an exchanger, since, in the solid part longitudinal and transverse conduction are of similar magnitude. This is especially true in configurations where solid walls are not thin, as opposed to fin exchangers, where a simple thermal resistance model to couple inlet and outlet fluid compartments with solid diffusion is not precise enough.

In the recent years, growing efforts have been dedicated to elaborate micro-heat exchangers for the design of micro-cooling systems associated with high power density micro-chips [3,13,5,6]. Compactness, effectiveness, and performance are indeed alltogether crucial in many contexts and different strategies have been proposed to search for optimal designs (e.g. [34,2,43,11,8]).

Furthermore, in the context of bio-heat transfer modeling of tissue convection within parallel vessels has been considered in many contributions, e.g. [42,44,16,32].

Since, generically, the local transfer rate from the fluid into the solid is found to abruptly decay from the inlet along the longitudinal direction [6,37], a strong emphasis has to be made upon the influence of the inlet and outlet conditions. To be more specific, in many cases a fully developed thermal boundary outlet condition is chosen [39,41,35,36,28,37] to model downstream convection. This is consistent with convective dominated situations with very large Péclet numbers. For more moderate Péclet numbers, a more elaborate coupling of the exchanger with the inlet/outlet is needed to properly take into account the influence of the convection leak inside the outlet, as well as the possible upstream backconduction in the inlet.

The aim of this contribution is to further explore the influence of inlet/outlet coupling and longitudinal diffusion onto a counter-current exchanger both in the balanced and unbalanced configuration. Whilst it is now easy to perform specific full-3D direct numerical computation with finite volume/finite element/finite differences methods (e.g [6,37]) for a given set of parameters and geometry, it is not yet simple to fully explore the parameter space influence as well as the coupling with inlets/outlets. The latter is especially true since highly convective situations are associated with downstream stretched-out longitudinal temperature gradients inside the outlets, scaling linearly with the Péclet number, so that a full discretization of this compartment is just not worth considering. In this contribution, since we use a generalized Graetz-mode decomposition, all the longitudinal variations are analytically known and do not necessitate any numerical discretization. Solving a two-dimensional numerical problem only and mapping it to a three dimensional one, offers a powerful tool to explore parameter space. Most of the numerical method used in this paper has been detailed in a previous contribution [24]. Hence we will not repeat the method's technical details here in order to lighten the reading of the manuscript. We will rather concentrate on discussing the significance and interest of the obtained results from a physical viewpoint. Most technical aspects related to the mathematical formulation are given in Appendix A.1. The mathematical justification of the method in the context of Robin–Fourier (convective) lateral boundary condition on the exchanger will be worth considering in the future. In this contribution we provide a complete and accurate parameter exploration of counter-current exchangers coupled with their inlet/outlets at very moderate numerical cost, in order to extract the most salient features of the transfer.

In Section 2 the set of governing equations and their dimensionless formulation are provided. Some insights about the Graetz mode decomposition, and the boundary condition issue are discussed. In Section 3 the effectiveness and transfer estimate are discussed as well as a detailed description of the exchanger geometry under study. Section 4 describes the analysis of the exchanger performance from considering dimensionless Nusselt number and effectiveness ratio on balanced counter-current configuration when varying the Biot number, a dimensionless Péclet number, conductivity ratio, and exchanger length. Some unbalanced cases are also analyzed at the end of this section. In Section 5 we discuss the obtained results in the light of fully developed Graetz mode analysis, and provide simple generic behavior of convective dominated exchangers.

2. Governing problem and dimensionless formulation

2.1. Exchanger geometry

We consider laminar convection–diffusion arising in a fluid having constant properties. In the following we assume that the hot and cold tubes are filled with the same fluid, although this simplifying assumption is not a restriction of the proposed approach. Fully developed solutions of Navier–Stokes momentum equations in cylindrical tubes oriented along direction z are given by the Poiseuille longitudinal velocity $\mathbf{v}_H = v_H(r)\,\mathbf{e}_z = 2V_H\left(1-(r/R)^2\right)\mathbf{e}_z$and $\mathbf{v}_C = v_C(r)\,\mathbf{e}_z = -2V_C\left(1-(r/R)^2\right)\mathbf{e}_z$where V_H — respectively V_C — stands for the average velocity in the hot — respectively cold — tube, where R is the tube radius and $\mathbf{e}_z$ is the unit vector along z direction. The hot tube refers to the tube with homogeneous inlet temperature at minus infinity $T_H^{-\infty}$ and the cold tube refers to the tube with homogeneous inlet temperature at plus infinity $T_C^{+\infty}$ as represented on Fig. 2.

In most of the following we will consider the special case of a balanced counter-current configuration where longitudinal velocities are identical $V_H = V_C = V$ whilst using the same fluid in the hot and cold tubes. But, we also explore the case of an unbalanced exchanger where the fluxes and velocities are different, as detailed in forthcoming sections. For any aspect of the proposed approach one could have chosen any tube shape as explained in [24]. Here, we study the special case of cylindrical sections of the inlet/outlets but we will qualitatively comment in Section 5 about the generalization of the obtained results to other shapes.

Studying the influence of exchanger geometry on transfer performance has been the object of intense research especially in the context of compact micro-exchangers or bio-heat transfer in tissues where counter-flow configurations are also relevant to many bio-heat problems. Quoting [31], 'since a considerable fraction of blood vessels are found in pairs vessel-vessel heat transfer has generally been postulated as one of the most important heat transfer mechanisms involved in determining the tissue temperature distributions' [20,14,45].

Since this study focused on into the analysis of the influence of physical, thermal and hydraulic parameters, which already represent six independent dimensionless parameters, we shall not study the influence of the geometry on transfer. We arbitrarily set-up a simple tubular shape geometry as described in Figs. 1–3. Two counter flow tubes separated by a distance $d = R$. The radius of the exchanger is $R_E = 4R$ where R is also the radius of the flow tubes. This configuration is very similar with the ones considered in [4,44,31,16,10] where parallel tubes in counter-current vessels within tissue are considered.

It is interesting to mention that the surface to volume ratio of our exchanger is $2(2\pi R)/\pi(4R)^2 = 1/4R$ whilst the surface ratio between fluid and solid is $2\pi R^2/\pi(4R)^2 = 1/8$. Hence eventhough the solid surface represents eight times the fluid one, the

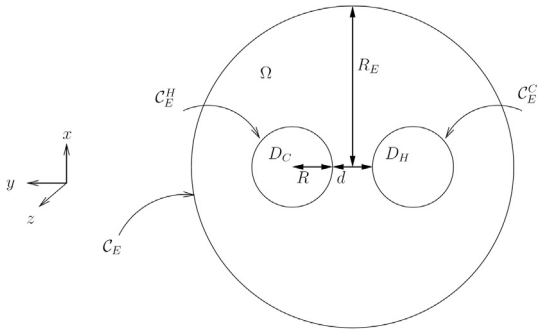

Fig. 3. Schematic layout of the transverse section of the heat exchanger. We have set $R_E = 4R$ and $R = d$.

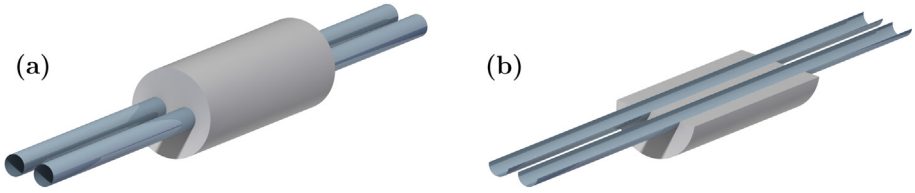

Fig. 1. Perspective view using real size of (a) full exchanger (b) opened half-exchanger where the fluid tubes inside the exchanger are visible.

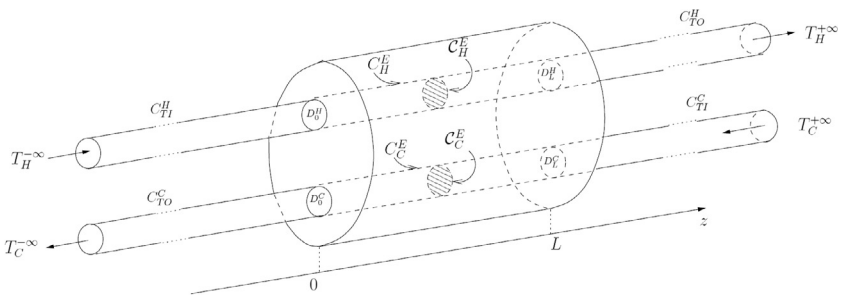

Fig. 2. Schematic layout of the exchanger geometry defining the various notations associated with the interface between tubes and exchangers, as well as the edges of the various components.

compactness (surface to volume ratio) can reach high values as tube diameters are decreased. For millimeter radius inlet tubes this ratio reaches value close to 250 m^{-1}, and for one tens millimeter radius 2500 m^{-1}, which are to be compared with what is usually considered as 'compact' exchangers for where the ratio is 700 m^{-1} [30].

Changing the radius not only increases the compactness but it also decreases the Péclet number. We will see in the following that this turns-out to be very interesting for effectiveness.

2.2. Governing problem

We write the stationary thermal energy balance in three dimensions as

$$\begin{aligned} &\rho c \mathbf{v}\cdot\nabla T - k^F \Delta T = 0 \text{ in } \quad \text{Fluid} \\ &k^S \Delta T = 0 \text{ in } \quad \text{Solid} \end{aligned} \tag{1}$$

with k^F & k^S being the Fluid and Solid thermal conductivity, ρ the fluid density and c the heat capacity; the above problem reads more explicitly for longitudinally invariant velocity convection $\mathbf{v} = v(x,y)\,\mathbf{e}_z$ as

$$\begin{aligned} &\rho c\, v(x,y)\partial_z T - k^F\left(\partial_x^2+\partial_y^2+\partial_z^2\right)T = 0, \quad \text{in} \quad \text{Fluid} \\ &k^S\left(\partial_x^2+\partial_y^2+\partial_z^2\right)T = 0, \quad \text{in} \quad \text{Solid} \end{aligned} \tag{2}$$

We denote C^E, the lateral surface of the exchanger, and C_H^E & C_C^E the hot & cold tube surface inside the exchanger. C^E, C_H^E and C_C^E are all cylinders localized in the longitudinal direction between 0 and L. We consider a Robin-Fourier convective lateral boundary condition, on cylinder C^E whose base is circle $\mathcal{C}^E$, $C^E = \mathcal{C}^E \times [0,L]$,

$$-k_S \partial_n T|_{C^E} = h(T|_{C^E} - T_a), \tag{3}$$

where T_a is the reference temperature in the air and h the heat transfer coefficient. We define the continuity condition inside the exchanger between the solid and the fluids interfaces C_H^E and C_C^E. Let us define $\partial\Omega_F = C_H^E \cup C_C^E$ and $\partial\Omega_S = \partial\Omega / C^E$ where $\partial\Omega$ is the full frontier of the solid domain and C^E is the exchanger cylinder (lateral frontier between the ambient air and the solid). Then continuity of temperature and fluxes read as

$$\begin{aligned} &T|_{\partial\Omega_F} = T|_{\partial\Omega_S} \\ &k^F \partial_n T|_{\partial\Omega_F} = k^S \partial_n T|_{\partial\Omega_S} \end{aligned} \tag{4}$$

where, at inlet and outlet tubes external boundaries C_{TI}^C, C_{TI}^H, C_{TO}^C and C_{TO}^H we consider homogeneous adiabatic Neumann boundary conditions for lateral edges,

$$\partial_n T|_{C_{TI}^C, C_{TI}^H, C_{TO}^C, C_{TO}^H} = 0. \tag{5}$$

At infinity, in the inlets the cold and hot sources temperatures are imposed

$$\begin{aligned} &T|_{D^H}(x,y,z\to-\infty) = T_H^{-\infty} \\ &T|_{D^C}(x,y,z\to+\infty) = T_C^{+\infty}, \end{aligned} \tag{6}$$

where D^H and D^C denote the disk on hot and cold tubes.

2.3. Dimensionless formulation

Following previous studies (e.g. [28]), let us now use dimensionless variables with $\star$ index defined as $x = Rx^\star$, $y = Ry^\star$, $z = Rz^\star$, $L = L^\star R$, $v_H = 2V_H v_H^\star$, $v_C = 2V_C v_C^\star$, and

$$T^\star = \frac{T - T_H^{-\infty}}{T_H^{-\infty} - T_C^{+\infty}} + \frac{T - T_C^{+\infty}}{T_H^{-\infty} - T_C^{+\infty}}. \tag{7}$$

Now, using the dimensionless position $\xi^\star = (x^\star, y^\star)$ in the (x,y) plane (2) reads

$$\begin{aligned} &Pe_{H,C}\, v^\star(\xi^\star)\partial_{z^\star} T^\star - \left(\partial_{x^\star}^2+\partial_{y^\star}^2+\partial_{z^\star}^2\right)T^\star = 0, \quad \text{in} \quad \text{Fluid} \\ &\left(\partial_{x^\star}^2+\partial_{y^\star}^2+\partial_{z^\star}^2\right)T^\star = 0, \quad \text{in} \quad \text{Solid} \end{aligned} \tag{8}$$

At the lateral exchanger external interface with air, one has the following boundary condition

$$-\partial_{n^\star} T^\star = Bi(T^\star - T_a^\star), \tag{9}$$

where we have now introduced an effective external dimensionless reference temperature

$$T_a^\star = \frac{T_a - T_H^{-\infty} - T_C^{+\infty}}{T_H^{-\infty} - T_C^{+\infty}}, \tag{10}$$

introducing the usual Biot number $Bi = hR/k_S$. Let us precise that all domains will be denoted with a star due to the nondimensionalization of space variables $x^\star$, $y^\star$, $z^\star$. At the interface $C_H^{E\star}$ & $C_C^{E\star}$ between the hot and cold fluid tubes and the solid inside the exchanger, one has continuity of temperature and fluxes

$$\begin{aligned} &T^\star|_{\partial\Omega_F^\star} = T^\star|_{\partial\Omega_S^\star} \\ &k^F \partial_n T^\star|_{\partial\Omega_F^\star} = k^S \partial_n T^\star|_{\partial\Omega_S^\star}. \end{aligned} \tag{11}$$

Due to the choice of dimensionless temperature the imposed cold and hot sources verify

$$\begin{aligned} &T^\star|_{D^{H\star}}(\xi^\star, z^\star\to-\infty) = T_H^{\star-\infty} = 1, \quad \text{in Hot inlet} \\ &T^\star|_{D^{C\star}}(\xi^\star, z^\star\to+\infty) = T_C^{\star+\infty} = -1, \quad \text{in Cold inlet,} \end{aligned} \tag{12}$$

Dimensionless formulation thus brings six different dimensionless parameters: two hot and cold Péclet numbers $Pe_{H,C} = 2\rho c V_{H,C} R/k_F$, the Biot number Bi, the conductivity ratio between the solid and the fluid k^S/k^F, the effective external dimensionless reference temperature $T_a^\star$ defined in (10), and the exchanger aspect ratio $L^\star = L/R$. In the following we will mainly focus on the situation of balanced counter-flow exchanger for which $Pe_H = Pe_C = Pe$ and systematically study the influence of the Biot parameter Bi, the exchanger aspect ratio $L^\star$ and conductivity ratio k^S/k^F.

2.4. General comments on the formulation and numerical method

It is important to mention that the outlet temperature in hot or cold tubes are not known a priori because convection–diffusion exchanger problems do not prescribe the outlet conditions. This is a very important point since, in the general case of arbitrary (and possibly moderately convective situations) Péclet number regime, outlet conditions at the exchanger frontier, D_L^H & D_O^C, are needed for the problem to present a closed form, and thus to get a proper numerical solution. In most of the previous literature on the subject, since most investigators were interested in the convective limit for which convection dominates over diffusion, the outlet boundary conditions where not necessary for the problem to be solved. Since most exchangers designed for practical applications where considered in the $Pe \gg 1$ regime, for which the Nusselt number is the largest, this approximation was consistent.

Here, we wish to analyze the general problem associated with any Péclet number, and thus some outlet conditions are necessary to get a solution.

It was shown and discussed in detail in [25,24] that the exchanger outlet conditions can not be decoupled from the tube outlet temperature field, and that all inlet–outlet-exchanger compartments are to be solved together in order to find a proper solution.

Even though considering a coupled problem which includes inlet and outlet drastically simplifies the question concerning the outlet condition, since at infinity the outlet temperature field is uniform within D^C & D^H, so that only two constants $T_C^{\star-\infty}$ & $T_H^{\star+\infty}$ are to be found, (for balanced counter-flow exchangers only one constant is enough), these constants are still missing! Hence, these constants need to be settled as unknowns of the problem and solved together with it. This is what is done here following [24], so that we do not develop further the detailed numerical formulation. Since this paper does not focus on the method, but rather on the obtained results, the interested reader should get a more precise description of the numerical method used in [24]. Nevertheless, Appendix B presents a brief description of the numerical implementation of the method. Following [24] the numerical solution is based upon a generalized Graetz mode decomposition of the problem in each compartment

$$
\begin{aligned}
&T^\star(\xi^\star,z^\star)=\sum_{\mathbb{N}^*}x_n^+T_n^+(\xi^\star)e^{\lambda_n^+z^\star}+x_n^-T_n^-(\xi^\star)e^{\lambda_n^-(z^\star-L^\star)}\\
&\quad\text{exchanger } z^\star\in[0,L^\star]\\
&T^\star(\xi^\star,z^\star)=x_0^H+\sum_{\mathbb{N}^*}x_nt_n^+(\xi^\star)e^{\mu_n^+(z^\star-L^\star)}\\
&\quad\text{hot outlet tube } z^\star\geqslant L^\star\\
&T^\star(\xi^\star,z^\star)=x_0^C+\sum_{\mathbb{N}^*}x_nt_n^-(\xi^\star)e^{\mu_n^-z^\star}\\
&\quad\text{cold outlet tube } z^\star\leqslant 0\\
&T^\star(\xi^\star,z^\star)=T_H^{\star-\infty}+\sum_{\mathbb{N}^*}x_nt_n^-(\xi^\star)e^{\mu_n^-z^\star}\\
&\quad\text{hot inlet tube } z^\star\leqslant 0\\
&T^\star(\xi^\star,z^\star)=T_C^{\star+\infty}+\sum_{\mathbb{N}^*}x_nt_n^+(\xi^\star)e^{\mu_n^+(z^\star-L^\star)}\\
&\quad\text{cold inlet tube } z^\star\geqslant L^\star
\end{aligned}
\tag{13}
$$

where $x_n^\pm$ are the amplitudes of the generalized Graetz modes, $T_n^\pm$ are the upstream and downstream exchanger Graetz modes, $\lambda_n^+<0$ are the upstream Graetz eigenvalues and $\lambda_n^->0$ are the downstream eigenvalues. $t_n^\pm$ are the upstream and downstream Graetz modes in the inlet and outlet tubes, $\mu_n^+<0$ are downstream Graetz eigenvalues in outlet tubes $\mu_n^->0$ are upstream Graetz eigenvalues in inlet tubes.

From knowing in each compartment, the inlet, outlet and the exchanger, that the solutions can be decomposed into a family of orthogonal modes, we are able to set the coupling conditions for these compartments to provide the proper matching of temperature and fluxes at their interfaces D_0^H, D_0^C, D_L^H, D_L^C. Using flux and temperature differences at interfaces D_0^H, D_0^C, D_L^H, D_L^C to be minimized as a cost functional, we are able to set a linear system for the generalized Graetz mode amplitude to be solved. This linear system includes the outlet modes amplitude which are, in fact, the two constants $T_C^{\star-\infty}$ & $T_H^{\star+\infty}$.

These constants are important since they define the effectiveness of the exchanger that we now recall.

3. Exchangers performances

3.1. Effectiveness

First we study the heat effectiveness of the transfer from considering

$$
\begin{aligned}
\epsilon_H&=\frac{T_H^{\star-\infty}-T_H^{\star+\infty}}{T_H^{\star-\infty}-T_C^{\star+\infty}}\\
\epsilon_C&=\frac{T_C^{\star-\infty}-T_C^{\star+\infty}}{T_H^{\star-\infty}-T_C^{\star+\infty}},
\end{aligned}
\tag{14}
$$

the usual hot and cold heat extraction dimensionless estimate. In the case of a balanced counter-flow configuration, those two quantities are exactly equal. This necessitates balancing Péclet numbers (when the fluids properties are identical in the hot and the cold tubes, the Péclet numbers are identical) inside both inlet and outlet tubes in the case of a lateral Robin-Fourier boundary condition as is considered here. It is interesting to note that when constant temperature T_w is applied at the lateral boundary which is equivalent to the limiting case of infinite Biot number $Bi\to\infty$ one can use a simple linear transformation of the temperature field relative to the imposed T_w at the boundary (i.e $T-T_w/(T_H^\infty-T_C^{+\infty})$) to obtain a balanced exchanger, for which the hot and cold efficiencies are identical, as previously considered in [24]. In the following we will only consider transformation (7) which permits to map any inlet thermal condition onto a balanced one.

3.2. Transfer

We mainly evaluate the transfer performance of the exchanger through the total hot –resp. cold– Nusselt number which is based upon the dimensionless total heat transfer from the hot –resp. cold– tube into the solid inside the exchanger integrated along the tube surface, and the dimensionless inlet's temperature difference

$$
Nu_{H,C}^{loc}=\frac{2Rh_{H,C}}{k^F}\ \text{with}\ h_{H,C}=\frac{-k^F\nabla T|_{\mathcal{C}_{H,C}^E}\cdot\mathbf{n}}{T_H^{-\infty}-T_C^\infty}
\tag{15}
$$

which leads to the dimensionless formulation of the Nusselt number

$$
Nu_{H,C}^{loc}=\left|-2\,\partial_{n^\star}T^\star\right|
\tag{16}
$$

One can then define the global Nusselt number by integrating over the hot –resp cold– tube,

$$
Nu_{H,C}=2\int_0^{L^\star}dz^\star\int_{\mathcal{C}_{H,C}^E}\partial_{n^\star}T^\star d\mathcal{C}_{H,C}^E.
\tag{17}
$$

Obviously, in the zero Biot number limit, since the problem is anti-symmetric, $Nu_H=Nu_C$. From using the generalized Graetz mode decomposition for the temperature field in the exchanger given in (13) one is able to analytically integrate along the longitudinal direction to obtain the Nusselt number versus some average quantities from using governing Eq. (8) and divergence theorem, so as to obtain

$$
\begin{aligned}
Nu_{H,C}=2Pe\int_{\mathcal{D}^{H,C}}v^\star(\xi^\star)\left[T^\star(\xi^\star,L^\star)-T^\star(\xi^\star,0)\right]d\xi^\star\\
-\int_{\mathcal{D}^{H,C}}\left[\partial_{z^\star}T^\star(\xi^\star,L^\star)-\partial_{z^\star}T^\star(\xi,0)\right]d\xi
\end{aligned}
\tag{18}
$$

We will use later on this expression in order to get a simplified expression of the Nusselt number in the fully developed limit in Section 4.3.

4. Results

We mainly consider cases where the ambient temperature is much smaller than the hot source so we set $T_a^\star=0$. We should stress that this limit should rather be considered in the light of dimensionless convective boundary condition (9) where one can

realize that the approximation is relevant when $T_a^\star \ll 1$. Nevertheless, this limit is not a limitation of the presented approach but is useful to shorten the parameter space and some example of order one $T_a^\star$ configurations are studied in Section 4.2.

4.1. Effectiveness of balanced counter-flow exchanger

We first consider the situation where $Pe_H = Pe_C = Pe$ so that the exchanger experiences a balanced counter-flow regime. We recall that due to the dimensionless temperature chosen, the dimensionless hot and cold sources temperatures are anti-symmetric and verify $\frac{T_H^{\star-\infty}}{T_C^{\star\infty}} = -1$. We will discuss at the end of the next section that the deviations from balanced prediction for the effectiveness resulting from non-symmetrical inlet conditions, at finite Biot number are of order $O(Bi)$. Such corrections to the adiabatic limit $Bi = 0$ are not trivial since non-linear higher order corrections are in fact expected. This comes from the fact that, for balanced configurations, a regular asymptotic expansion of the temperature solution of the form

$$T^\star = T^{(0)\star} + \sqrt{Bi}T^{(1)\star} + BiT^{(2)\star} + Bi^{3/2}T^{(3)\star} + \cdots \tag{19}$$

is indeed expected, where $T^{(0)\star}$ is the temperature solution associated with the adiabatic limit, for which the associated effectiveness is ϵ^0. This expansion is more precisely justified in Appendix A.2, where it is also shown that, for balanced configurations, each generalized Graetz mode and eigenvalue also reads

$$\begin{aligned} T_n &= T_n^{(0)} + \sqrt{Bi}T_n^{(1)} + BiT_n^{(2)} + Bi^{3/2}T_n^{(3)} + \cdots \\ \lambda_n &= \lambda_n^{(0)} + \sqrt{Bi}\lambda_n^{(1)} + Bi\lambda_n^{(2)} + Bi^{3/2}\lambda_n^{(3)} + \cdots \end{aligned} \tag{20}$$

Following this regular asymptotic expansion of the temperature, the effectiveness also admits a similar non trivial regular expansion, such that,

$$\epsilon = \epsilon^0 + \sqrt{Bi}\epsilon^1 + Bi\epsilon^2 + Bi^{3/2}\epsilon^3 + \cdots$$

It turns out that the leading order correction to ϵ^0 is indeed ϵ^2, for ϵ^1 to be zero. Furthermore, the above mentioned $O(Bi)$ correction to the effectiveness is only the leading order, so that, if needed, one could also evaluate each consecutive term of the sequence to find the resulting polynomial corrections to the effectiveness. In the following we will compute numerically the effectiveness, but consistently verify it fits within this asymptotic framework. Since deviations from balanced prediction are small when $Bi \ll 1$, we mainly focus our interest to the symmetrical inlet conditions in this section. Incidentally, as a side technical remark, it is interesting to mention that anti-symmetry of upstream and downstream generalized Graetz eigenvalues is only determined by the convective ratio condition $Pe_H = Pe_C = Pe$ and not by the imposed inlet thermal conditions defined by $T_a^\star$ which can be set arbitrarily without indeed changing the symmetry of the eigenmodes.

Hence, we first concentrate here on the influence of the Péclet number Pe, the conductivity parameter k^S/k^F, the Biot number Bi and the exchanger dimensionless length $L^\star$.

Let us consider the adiabatic limit for a very small Biot number. It is first interesting to emphasize that the reason for considering a very small Biot number (e.g as small as $Bi = 10^{-6}$) rather than the limit $Bi = 0$ is to properly approach the adiabatic limit numerically. Indeed the limit $Bi \to 0$ is problematic since the two $n = 0 \pm$ eigenmodes goes to zero, i.e $\lambda_0^\pm \to 0$, at this point so that the linear system (B.6) becomes singular. One possible way to circumvent this issue should be to remove those modes from the analysis, as done in singular value decomposition inversion methods. Nevertheless these two $n = 0$ modes do matter, since the transfer properties are controlled by them! Hence, the adiabatic limit is safely approached numerically from considering a small Biot number.

Fig. 4a shows the exchanger effectiveness when the Péclet number is varied for various dimensionless length $L^\star$. All effectiveness curves display a similar behavior, with three distinct regimes: (*i*) a small increase at low Péclet numbers followed by (*ii*) an optimal effectiveness arising at moderate Péclet, and (*iii*) a monotonous decrease arising at large Péclet. It is worth mentioning that, as expected, the effectiveness improves as dimensionless length $L^\star$ increases, as shown in Fig. 4b, since the longer the exchanger, the better the transfer. Nevertheless, it is obvious that reaching $L^\star$ values larger than one hundred does not present good practical perspectives, for obvious cost and caliber limitations. Considering the moderately elongated exchanger where $L^\star = 10$, it is striking to observe how poorly efficient such an exchanger can be for Péclet numbers not larger than one hundred, whilst in most practical situations the Péclet reaches much larger values (as large as several thousand at least). This statement has to be tempered with the fact that the hereby chosen exchanger geometry is obviously very far from the most efficient one. Obviously the larger the Péclet the larger the exchanges as later-on examined from the analysis of the

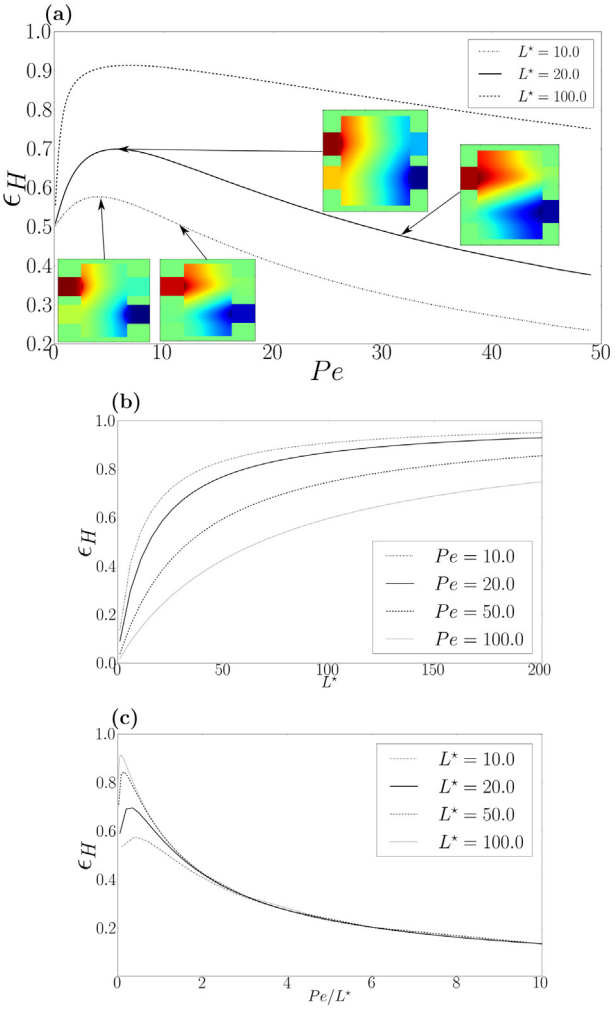

Fig. 4. In the three figures $Bi \ll 1$, $\frac{k^S}{k^F} = 1$. (a) ϵ_H against Péclet for $L^\star = 10,\ 20,\ 100$. Inset figures represent the computed longitudinal temperature fields at the maximum hot effectiveness as well as when the convective leak is starting to rise. It is important to stress that the aspect ratio of the figure is not the actual one for obvious caliber constraints. We have re-scaled the horizontal $z^\star$ axis in order the inset figures to reach a 1:1 aspect ratio, (b) ϵ_H against $L^\star$ for $Pe = 10,\ 20,\ 50,\ 100$, (c) ϵ_H against Péclet re-scaled by $L^\star$ for $L^\star = 10,\ 20,\ 50,\ 100$.

Nusselt number. Fig. 4c also provides some interesting insets representing the temperature field in the $(y^\star, z^\star)$ plane (rescaled along the $z^\star$ direction to keep with a 1:1 aspect ratio of the insets) illustrating the origin of the effectiveness collapse. As the Péclet is increased, a larger fraction of the initial hot inlet temperature is progressively converted toward the outlet, without having the chance to be transferred into the cold one through conduction within the solid. This convective heat-leakage across outlets is the mechanism by which the exchanger effectiveness is inevitably degraded as one increases convection for raising total heat transfer. Furthermore, for the range under study, the effectiveness curves of various exchanger designs having different aspect ratios $L^\star$ are found to collapse at large Péclet as illustrated in Fig. 4a from using the classical Graetz re-scaling $Gr = Pe/L^\star$. We will further discuss this collapse in Section 4.3 from reaching the fully developed limit.

Fig. 5a–d illustrate the influence of the conductivity ratio when the solid has either comparable or larger diffusivity compared to the convected liquid. In most applications (e.g. using solid metals), the solid is indeed a better heat conductor than fluid. The observed transverse heat profile at the exchanger longitudinal middle plane $(z^\star = L^\star/2)$ shows distinct regimes. For identical conductive properties in the fluid and the solid, i.e $k^S/k^F = 1$, the observed transverse gradients are spread all around the fluids tube inside the solid (with anti-symmetric shape in the $(x^\star, y^\star)$ plane in this balanced configuration). This illustrates that transverse diffusion in the solid arises, in this case, with transverse variation along distances of the order of the tube diameters. On the contrary, in Fig. 5b–d as k^S/k^F increases, the transverse conduction gradients in the solid shortens its typical length-scale variations to become more and more localized in the vicinity of the tubes frontiers $C^E_{H,C}$, leaving an almost iso-thermal temperature field within all the solid. Fig. 5e then shows that the optimal effectiveness is reached in the limit of large k^S/k^F. The small difference which is observed for the effectiveness curve between the case $k^S/k^F = 10^2$ and $k^S/k^F = 10^3$ indicates that there is an asymptotic maximum effectiveness associated with the limit $k^S/k^F \to \infty$. Both the iso-thermal behavior in the solid and the increasing effectiveness with increasing k^S/k^F ratio where to be expected. The more conductive the solid, the better the heat exchange between the fluids. It is worth mentioning that Maranzana et al. [12], found a conductivity ratio with optimal efficiency in a parallel plane convective exchanger. However, their study only investigates the single Péclet $Pe = 33$ value and also neglects longitudinal diffusion in the fluid which might explain their results. Furthermore, the configuration under study in [12] was different from ours since the solid domain was larger than the fluid one. In our configuration, even for extremely large k^S/k^F ratios, the three regimes (*i*,*ii*, *iii*) are also recovered in Fig. 5e. This indicated that even though the solid is an extremely good conductor, the convective conditions (associated with *Pe* number) and the exchanger aspect ratio $L^\star$ are

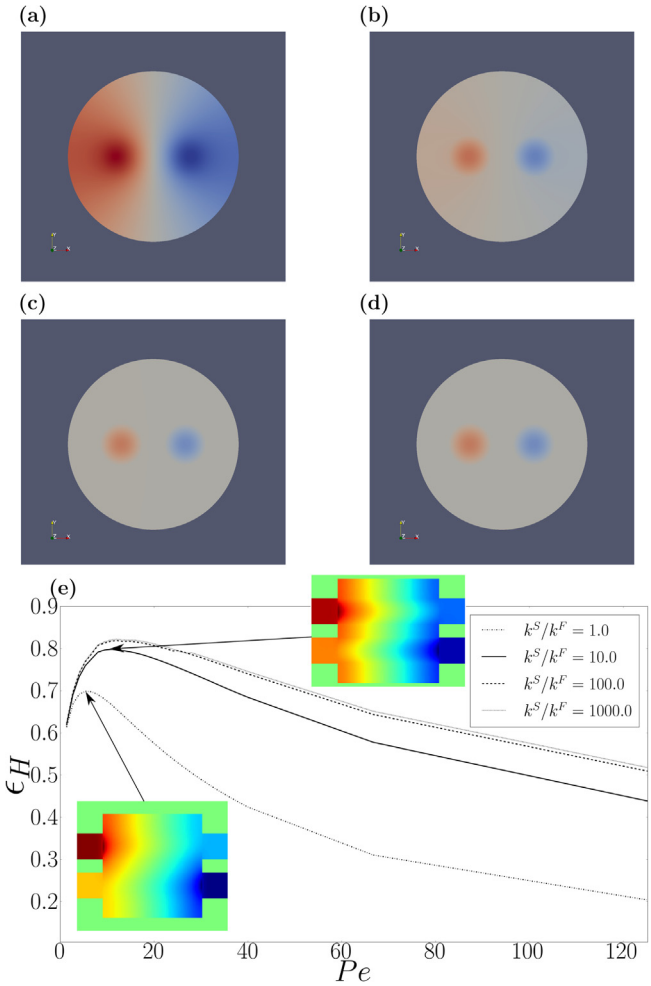

Fig. 5. Transverse temperature fields in exchanger at $z^\star = \frac{L^\star}{2}$ for $L^\star = 20$, $Bi = 10^{-6}$ and (a) $k^S/k^F = 1$, (b) $k^S/k^F = 10$, (c) $k^S/k^F = 10^3$, (d) $k^S/k^F = 10^4$. (e) ϵ_H against Péclet for $k^S/k^F = 1,\ 10,\ 100,\ 1000$ and $L^\star = 20$, $Bi = 10^{-6}$. Longitudinal temperature fields have been computed at the maximum hot effectiveness. $z^\star$ axis has been re-scaled in order for the inset figures to reach a 1:1 aspect ratio

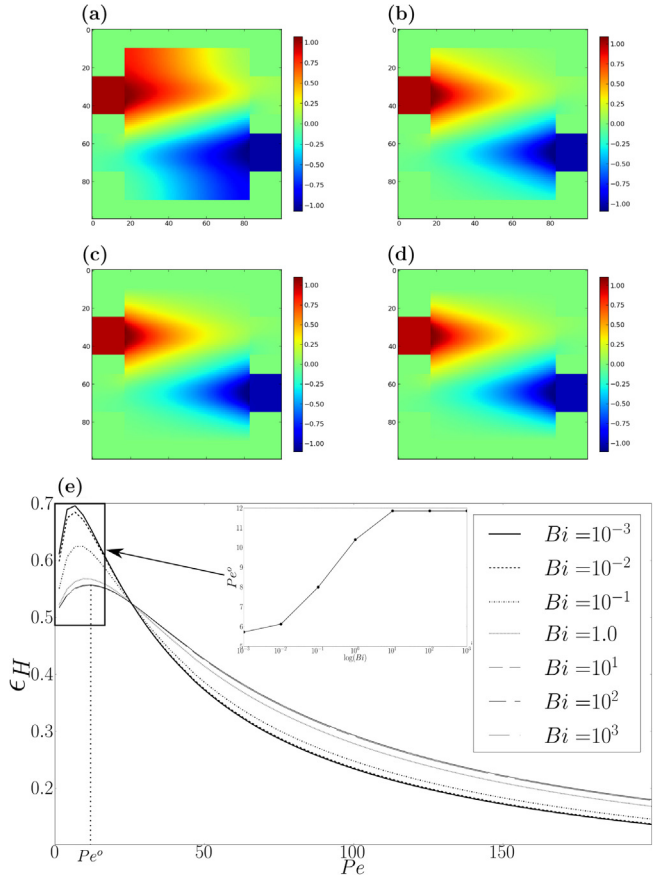

Fig. 6. Longitudinal temperature fields at $Pe = 25$, $L^\star = 20, \frac{k^S}{k^F} = 1$ for (a) $Bi = 10^{-3}$, (b) $Bi = 1$, (c) $Bi = 10$, (d) $Bi = 10^3$. (e) ϵ_H against Péclet for $L^\star = 20$ and $Bi = 10^{-3},\ 10^{-2},\ 10^{-1},\ 1,\ 10^1,\ 10^2,\ 10^3$. Inset figure is Péclet at maximum hot effectiveness against $\log(Bi)$.

driving the effectiveness. Furthermore it is very interesting to observe that the optimal effectiveness arising at moderate *Pe* number is almost insensitive to the conductivity ratio parameter.

Turning to the analysis of larger Biot number, we found a very weak influence of convective boundary on the previous heat-transfer regimes (*i*,*ii*,*iii*). In this paragraph, we first consider the case $T_a^\star = 0$. Fig. 6a–d illustrate the influence of the convective parameter *Bi* for an elongated exchanger $L^\star = 20$, with moderate convection $Pe = 25$ where one can observe that, in the vicinity of the external exchanger boundary $\mathcal{C}^E$ the temperature profile displays distinct regimes (here again the temperatures profiles have been re-scaled along the $z^\star$ direction to keep with a 1:1 aspect ratio of the figure).

At low Biot number $Bi \ll 1$, in Fig. 6a displays an adiabatic (homogeneous Neumann) behavior where the temperature isovalues are perpendicular to the $\mathcal{C}^E$ boundary associated with transversely homogeneous variations. On the contrary, at large Biot numbers $Bi \gg 1$, in Fig. 6d, the longitudinal variations of temperature are very weak all along $\mathcal{C}^E$ which is similar to an imposed temperature at the boundary (Dirichlet like). Fig. 6e provides the effectiveness for a large range of Péclet numbers, where the three distinct regimes (*i*,*ii*,*iii*) are clearly visible. In the wide range of explored Biot numbers, i.e. between 10^{-3} and 10^3 the optimal effectiveness is surprisingly robust and poorly sensitive to the *Bi* value. The peak of effectiveness observed as the Péclet number varies, moderately broadens and gets very slightly translated. The Fig. 6 inset provides the optimal Péclet number versus *Bi*, and one can observe that it always arises for moderate values of Péclet in a very narrow interval between 6 and 12.

A similar optimum for effectiveness versus the Graetz numbers was previously reported in a parallel configuration in [15]. Nevertheless, [15]'s optimum is not peaked in such a narrow range of Péclet number as found here. Furthermore the optimum Graetz number found in [15] (from their Fig. 4) for conductivity ratio equal to 100, resp 1000 is 0.4 resp. 0.9. In our case, using the results of Fig. 5, for both 100 and 1000 conductivity ratio we found almost identical optimal Graetz numbers equal to 0.3. Even if the specific value at which some optimal transfer occurs differs from [15], such a difference is not surprising considering the fact that the exchanger geometry is different. Nevertheless, as noticed earlier in the comments of Fig. 5, for high conductivity ratio, i.e. larger than 10, k^S/k^F was found to have a limited effect. We believe this observation to be new and the consequence of properly taking care off longitudinal diffusion arising in the fluid. Furthermore since the optimal Péclet value lies in a narrow range where convection is moderate, its precise estimation should also necessitate axial diffusion in the fluid to matter.

The relevance of this observation has practical implications that we will discuss in Section 5.

4.2. Effectiveness of unbalanced counter-flow exchanger

Now considering the case where $T_a^\star \neq 0$, we chose a possibly relevant set of working temperatures (for water) by choosing $T_H^{-\infty} = 353.15$ K, $T_C^{+\infty} = 283.15$ K and $T_a = 293.15$ K. From using (10) with the hereby given values of inlets and ambient temperatures we found $T_a^\star = -4.90$. Fig. 7 displays the behavior of hot (in red) and cold (in blue) effectiveness against Péclet variations for various small Biot numbers in the range 10^{-1}—10^{-6}. The values obtained for the effectiveness then indicate that in some cases it can be larger or smaller than one when the Biot number is not too small. This might be surprising at first, since one might think that effectiveness should always lie within $[-1, 1]$. Nevertheless, if one more closely evaluates the impact of the extra dimensionless ambient parameter $T_a^\star$ in boundary condition (9), it provides an extra heat-flux term which unbalances the exchanges between the inlet and the outlet. Hence, this extra-flux can lead to effectiveness out of the specific range $[-1, 1]$ for the heat in the hot fluid to be pumped further by the extra-flux term at the lateral boundary. As depicted in Fig. 7, depending on the Biot number, such an exchanger can either experience a systematic decreasing efficiency for increasing *Pe*, or a behavior showing maximal effectiveness at a moderate optimal Péclet number as found previously in the case $T_a^\star = 0$. Let us now turn to the case of unbalanced counter-flow configurations where $Pe_H \neq Pe_C$. Fig. 8 displays the hot and cold effectiveness curves when the hot and cold Péclet ratio varies. In the case of unbalanced configurations it is obviously expected that hot and cold effectiveness differ. Obviously, increasing convection in the hot tube will clearly increase the cooling from the hot tube but, reciprocally will level-down the heating of the cold fluid. This behavior of the exchanger is more systematically emphasized in Fig. 8 where the hot effectiveness (with crosses) is improved as Pe_H increases. Furthermore, at the same time the cold effectiveness of the exchanger drops down as Pe_H increases for a given Pe_H/Pe_C ratio. Depending on the application, it might be more interesting to favor either one or the other functions of the exchanger.

4.3. Transfer and fully-developed regime

As mentioned earlier, the larger the convection the larger the transfer, at the cost of low effectiveness. Fig. 9a displays the obtained Nusselt for a large range of Péclet numbers and exchanger aspect ratios $L^\star$. In these results one can clearly observe the influence of convective leakage inefficiency: e.g. for $L^\star = 5$ or $L^\star = 10$,

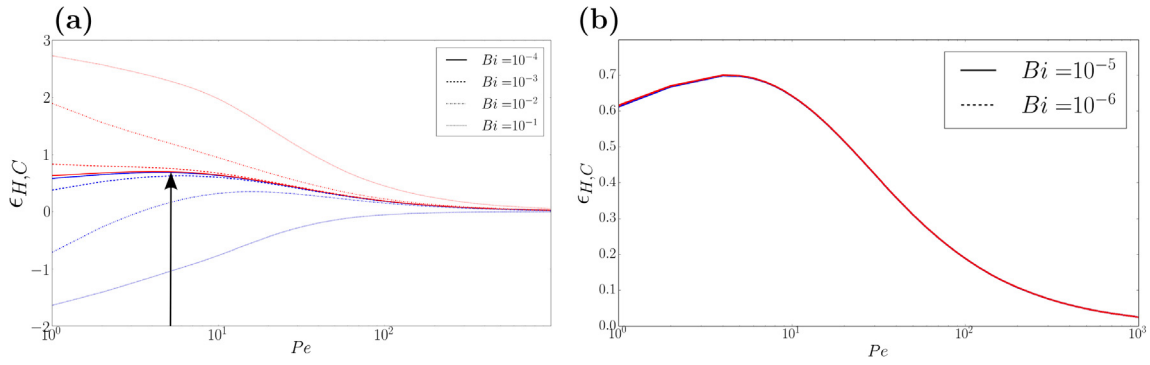

Fig. 7. Hot effectiveness (red) and cold (blue) effectiveness versus Péclet number *Pe* for a non-zero $T_a^\star = -4.90$ and various small Biot numbers (a) $Bi = 10^{-4}$, 10^{-3}, 10^{-2}, 10^{-1}, (b) $Bi = 10^{-5}$, 10^{-6} For sufficiently small Biot number an optimal effectiveness is recovered at a moderate Péclet number. (For interpretation of the references to color in this figure legend, the reader is referred to the web version of this article.)

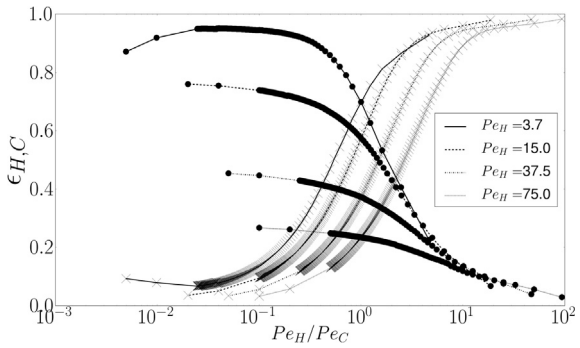

Fig. 8. ϵ_H in crosses and ϵ_C in full dots against Péclet ratio for $Pe_H = 3.7,\ 15,\ 37.5,\ 75$ and $L^\star = 20,\ Bi = 10^{-6},\ \frac{k^S}{k^F} = 1$.

the Nusselt number saturates to a plateau when the Péclet number gets larger than 50 or 100. Obviously the more elongated the exchanger the longer it takes to reach this plateau. However, there is an upper limit to $L^\star$ for which practical issues become a concern for caliber constraints. Hence convective leakage becomes a limitation to transfer, as convection is increased. Fig. 9b also displays the transfer variations as the conductivity ratio is varied. As discussed in Section 4.1, where we found that the effectiveness reaches an optimal value as the conductivity ratio between the solid and the fluid gets larger and larger, the transfer also reaches a maximal asymptotic curve as $k^S/k^F \to \infty$. But even in the most favorable case where $k^S/k^F \gg 1$, we still observe the inflection of the transfer increase, which saturates at very large Péclet due to the convective leakage.

As the best transfer comes at high Péclet, $Pe \gg 1$ and for very elongated $L^\star \gg 1$ configurations it is interesting to investigate specifically this limit. The collapse of the effectiveness curve presented in Fig. 4a in a previous section suggests that a special transfer regime is reached when convection dominates. Indeed, this limit produces a very nice simplification which generalizes the standard Graetz *fully developed* limit, for which effectiveness only depends on the Graetz number $Gr = Pe/L^\star$. In this limit only the first non-zero mode of the Graetz development matters inside the exchanger. Neglecting the second term of the numerator of expression (18), for being $O(1/Pe)$ smaller than the first one, whilst using Graetz decomposition (13) leads to

$$Nu_{H,C} = 2\,Pe\left(\sum_n x_n^+(e^{\lambda_n^+ L}-1)\langle T_n^+\rangle_c - \sum_n x_n^-(e^{-\lambda_n^- L}-1)\langle T_n^-\rangle_c\right), \quad (21)$$

with $\langle T\rangle_c = \int_{D_{H,C}} v^\star(\xi^\star)T^\star(\xi^\star)d\xi^\star$ the mixing cup temperature.

From the anti-symmetry of the Graetz modes and Graetz eigenvalues (see Appendix C), $\lambda_n^+ = -\lambda_n^-$, it follows

$$Nu_{H,C} = 2\,Pe\left(\sum_n (e^{\lambda_n^+ L}-1)\left(x_n^+\langle T_n^+\rangle_c - x_n^-\langle T_n^-\rangle_c\right)\right) \quad (22)$$

Now considering the main contribution of the two $\pm$ modes associated with $n = 0$, it can be checked numerically that for all $n \geqslant 1$, $(e^{\lambda_n^+ L}-1)\left(x_n^+\langle T_n^+\rangle_c - x_n^-\langle T_n^-\rangle_c\right) \ll (e^{\lambda_0^+ L}-1)\left(x_0^+\langle T_0^+\rangle_c - x_0^-\langle T_0^-\rangle_c\right)$ and that $x_0^-\langle T_0^-\rangle_c = -x_0^+\langle T_0^+\rangle_c$ which, in limit $Pe \gg 1$, leads to

$$Nu_{H,C} \approx 4\,Pe\,\lambda_0^+ L^\star x_0^+\langle T_0^+\rangle_c \quad (23)$$

Using the divergence theorem on the Eq. (A.6) associated with the mode T_0^+, in the large Péclet number limit $Pe \gg 1$ one gets

$$\langle T_0^+\rangle_c = \frac{\phi_0^+}{Pe\lambda_0^+} \quad \text{with} \quad \phi_0^+ = \int_{C_{H,C}^E} \partial_{n^\star} T_0^+\, dC_{H,C}^E. \quad (24)$$

This equation is supported by the numerical results depicted in Fig. 10. Indeed, Fig. 10a first illustrates the simple asymptotic behavior of the zeroth eigenvalue λ_0^+ at high Péclet, also supported by theoretical derivations in Appendix (A.2), i.e.

$$\lambda_0^+ \sim \frac{\sqrt{Bi}}{Pe}, \quad (25)$$

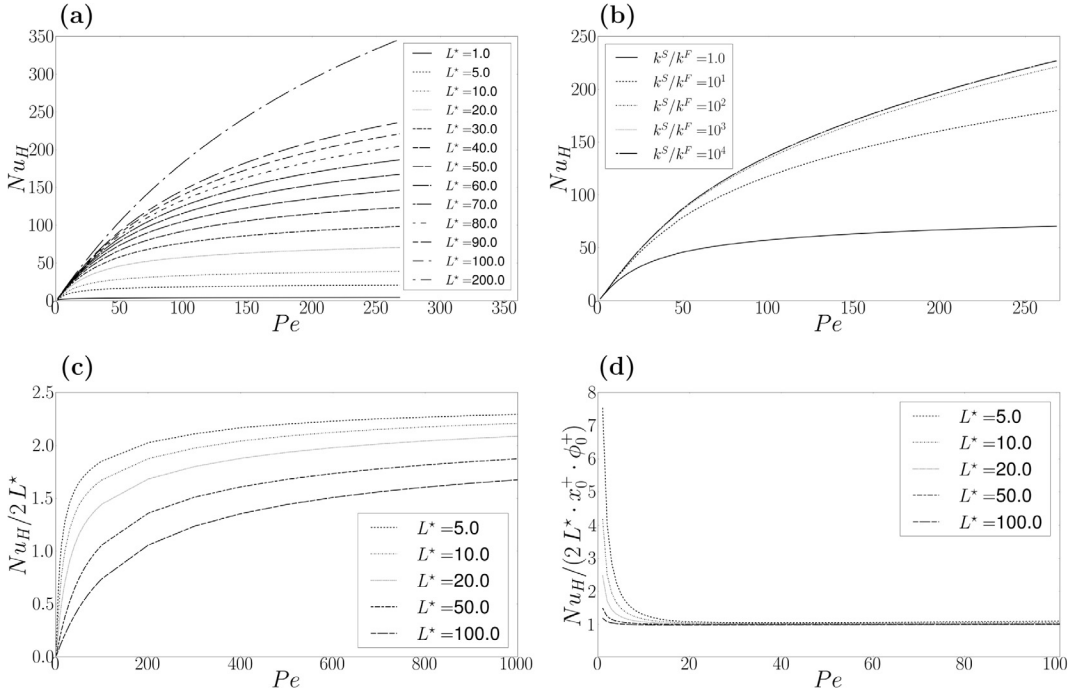

Fig. 9. (a) Nusselt against Péclet for $L^\star = 1,\ 5,\ 10,\ 20,\ 30,\ 40,\ 50,\ 60,\ 70,\ 80,\ 90,\ 100,\ 200$ and $Bi = 10^{-6},\ k^S/k^F = 1$, (b) Nusselt against Péclet for $k^S/k^F = 1,\ 10,\ 10^2,\ 10^3,\ 10^4$ and $Bi = 10^{-6},\ L^\star = 20$, (c) Nusselt rescaled by $2L^\star$ against Péclet for $L^\star = 5,\ 10,\ 20,\ 50,\ 100$ and $Bi = 10^{-6},\ k^S/k^F = 1$, (d) Nusselt rescaled by $2L^\star x_0^+\,\phi_0^+$ supporting asymptotic result (27) against Péclet for $L^\star = 5,\ 10,\ 20,\ 50,\ 100$, and $Bi = 10^{-6},\ k^S/k^F = 1$.

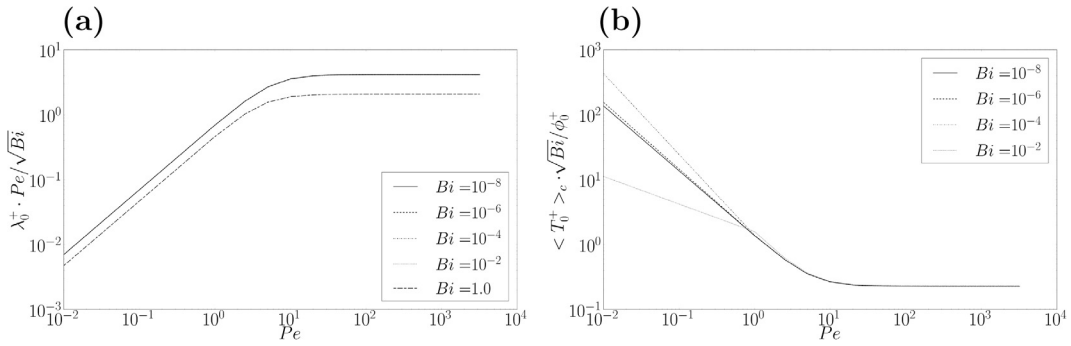

Fig. 10. (a) Bi-logarithmic plot of $\lambda_0^+ \cdot Pe/\sqrt{Bi}$ against Péclet for $Bi = 10^{-8},\ 10^{-6},\ 10^{-4},\ 10^{-2},\ 1,\ L^\star = 10$ and $k^S/k^F = 1$, For $Bi \ll 1$, and $Pe \gg 1$ a master curve illustrates the asymptotic scaling $\lambda_0^+ \sim \sqrt{Bi}/Pe$. (b) Bi-logarithmic plot of $\langle T_0^+ \rangle_c \cdot \sqrt{Bi}/\phi_0^+$ against Péclet for $Bi = 10^{-8},\ 10^{-6},\ 10^{-4},\ 10^{-2},\ L^\star = 10$ and $k^S/k^F = 1$. In the limit of $Bi \ll 1$, and $Pe \gg 1$ a master curve is obtained supporting scaling (26).

as similarly found for the $n = 1$ modes in the adiabatic case in [27]. Furthermore, Fig. 10b shows that numerical results give the following simple scaling for the leading order mode mixing-cup temperature,

$$\langle T_0^+ \rangle_c = \frac{\phi_0^+}{\sqrt{Bi}} \tag{26}$$

Using (25) in (26) leads to (24). Hence, the numerical results displayed in Fig. 10b provide a confirmation for the theoretical asymptotic behavior of the leading order mode. Finally the asymptotic global Nusselt number, in the limit $Pe \gg 1$ fulfills the following simple relation

$$Nu_{H,C} \approx 4 L^\star x_0^+ \phi_0^+ \tag{27}$$

Fig. 9d shows that this fully developed limit (27) arises when the Péclet number reaches values larger than 40, and is weakly dependent on the exchanger aspect ratio. This result is important for practical application since it shows that, for a convective dominated regime (which is not the more efficient one) a simple computation can provide a precise answer to the transfer rate, from using only the leading order mode. This *a posteriory* confirms the interest of considering optimal transfer configurations from analyzing the leading order mode only [8].

4.4. Effectiveness in the fully-developed regime

We now consider the exchanger effectiveness in the fully-developed regime. Considering the (hot) effectiveness $\epsilon_H = \frac{T_H^{\star -\infty} - T_H^{\star +\infty}}{T_H^{\star -\infty} - T_C^{\star +\infty}}$ in the dimensionless formulation, one gets

$$\epsilon_H = \frac{T_H^{\star -\infty} - 1}{2}. \tag{28}$$

Starting from Eq. (18) whilst considering the fully developed limit $Pe \gg 1$, for which, as in previous section, we neglect the second rhs term, one gets

$$Pe\left(\frac{\langle T^\star(0)\rangle_c - \langle T^\star(L^\star)\rangle_c}{Q_H^\star}\right) = \frac{Nu_H}{2Q_H^\star} \tag{29}$$

with $Q_{H,C}^\star = \int_{D_{H,C}} v^\star = \frac{\pi}{2}$. Consistently considering the fully developed limit, applying the divergence theorem in both the upstream and downstream hot pipe when using adiabatic lateral boundary conditions, one finds the following relations

$$\begin{aligned} \frac{\langle T^\star(0)\rangle_c}{Q_H^\star} &= T_H^{\star -\infty} = 1 \\ \frac{\langle T^\star(L^\star)\rangle_c}{Q_H^\star} &= T_H^{\star +\infty} \end{aligned} \tag{30}$$

Combining (28), (29), (30) gives the asymptotic relation between the effectiveness and the number of heat transfer units $Ntu_{H,C} = Nu_{H,C} L^\star/Pe$ to read as

$$\epsilon_H = \frac{Ntu_H}{4 Q_H^\star L^\star} \tag{31}$$

It is important to mention that the derivation of (31) propounding a linear relation between effectiveness ϵ_H and the number of heat transfer units Ntu_H has only been obtained from using asymptotic considerations and the divergence theorem. It thus applies to any parallel exchanger configuration, having any tube sections shape, any number of tubes, as well as for any exchanger section shape. This result indeed generalizes the result given in [15] for a parallel plate configuration. Fig. 11 displays the asymptotic behavior (31) for two exchanger lengths $L^\star = 10$ in (a) and $L^\star = 20$ in (b)

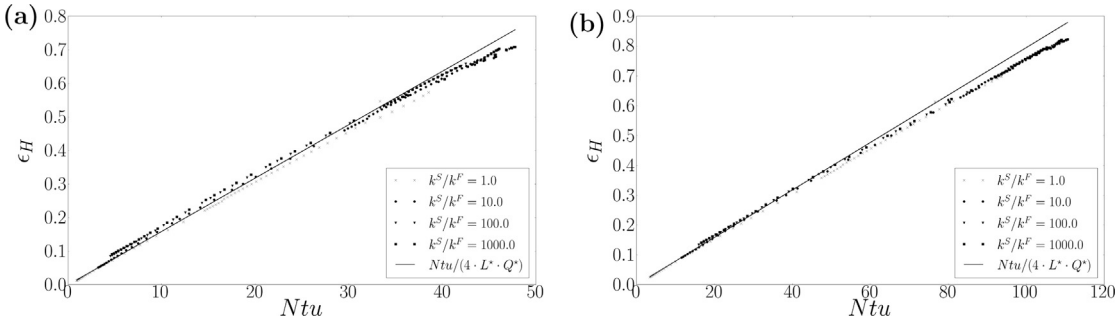

Fig. 11. Hot effectiveness ϵ_H versus Ntu for conductivity ratios $k^S/k^F = 1,\ 10,\ 100,\ 1000$ for (a) $L^\star = 10$, (b) $L^\star = 20$ exchangers. In both cases the solid line display the theoretical asymptotic prediction (31). Points are associated with full numerical computations.

compared with full numerical computations for various conductivity ratios $k^S/k^F = 1,\ 10,\ 100,\ 1000$. The comparison between the asymptotic results and the numerical computation is surprisingly good. In principle, only the limit of small to moderate *Ntu* (associated with $Pe \gg 1$) should be ruled by relation (31), whilst, for large *Ntu* (when *Pe* becomes of order one) prediction (31) is irrelevant. Indeed, one can observe in Fig. 11 that the larger $L^\star$, the better the linear trend as well as the collapsed points in the small *Ntu* limit. On the contrary, for larger values of *Ntu*, and obviously for largest effectiveness, a deviation to the linear trend is observed. The deviation is indeed modest, so that, (31) offers a surprisingly robust prediction. It must be pointed out that Mori et al. found in [15]'s Fig. 2 a local optimum depending on the number of heat transfer units, which we do not recover here. This might be explained by the fact that [15] indeed neglect the longitudinal diffusion in the fluid but not in the solid. Also, in the configuration studied in [15], the aspect ratio solid over fluid is much higher than in our case which might explain the existence of such an optimum.

5. Discussion and conclusion

A Dimensionless formulation of a counter-flow exchanger provides six different parameters: associated with the thermal, physical and mechanical parameters of the exchanger operating conditions. Focusing on the most relevant ones (i.e the Péclet number, the diffusivity ratio, the aspect ratio, the Biot number) we have found various generic properties which should generalize to many exchanger geometries, when inlet/outlet conditions are properly taken into account.

- Depending on the Péclet number, three regimes of exchanges have been found: (i) at low Péclet numbers, when increasing convection, the performances are also increasing, so that, (ii) at moderate Péclet numbers, an optimal effectiveness is reached, whilst (iii) at large Péclet number, strong performance degradation associated with convective leak have been found. The existence of convective leaks associated with performance degradation is expected for any inlet/outlet geometries when convection dominates.
- Optimal exchanges at moderate Péclet numbers are found very robust to changes in other parameters such as boundary conditions (Biot number) and diffusivity ratio. We believe that this result has important implications for applications in many other exchanger geometry. It is worth noting that the assumption of Poiseuille flow profile is not expected to qualitatively change most of the obtained numerical computations nor the asymptotic results in fully developed regime. It is related to a proper consideration of longitudinal and transverse diffusion in the fluid as well as in the solid. This supports the view that compact exchangers associated with moderate Péclet numbers provide the best effectiveness and are thus interesting for transfer performance at moderate cost for fluid pumping. This might also be the reason why, most biological exchangers associated with mass transfer from the vascular system into tissue, are operating at moderate Péclet numbers.
- At large Péclet numbers and for long exchangers, a 'fully developed' regime can be defined which generalizes the one known for the simple Graetz problem. In this regime, the Nusselt number is mainly determined by the first generalized Graetz mode having a simple linear dependence with the flux and amplitude of this mode. In this regime, we also generalize the asymptotic linear relation between the effectiveness and the number of heat transfer units Ntu_H for any parallel exchanger configuration and found it surprisingly robust when compared to numerical computation.
- Finally, for small Biot numbers, some generic behavior has also been studied. Even if, in parallel exchangers, the temperature as well as the generalized Graetz modes, and by consequence, the effectiveness are found to be *non-linear* functions of the Biot number, the $Bi \ll 1$ regimes display a $\lambda_0 \sim \sqrt{Bi}/Pe$ behavior of the first generalized Graetz eigenvalue. Furthermore, the leading order deviation of the effectiveness and exchanges from the pure adiabatic limit are $O(Bi)$.

It is worth mentioning that the Generalized Graetz approach that we have used can handle any tube shape and/or boundary conditions, as well as an arbitrary number of inlet/outlets. The numerical results have shown that the leading order mode mostly dominates the overall transfer when $Pe > 50$ so that a single 2D computation is mostly enough for providing a very good estimate of the transfer in many cases. Nevertheless, optimal performances are found at more moderate Péclet numbers where supplementary modes contribute.

Acknowledgement

We wish to thanks Jennifer Mackie for careful reading of the manuscript.

Appendix A. Theoretical properties of generalized Graetz modes

A.1. Formulation of generalized Graetz modes

In this section we recall the formulation of generalized Graetz modes, that have already been treated in [25,26,7]. The theoretical full proof with a lateral Robin boundary condition will be given in a future contribution. In this section, we will just recall how one can write the main problem as an ordinary differential equation. From Eq. (8), defining global velocity $\tilde{v}^\star$ as a function that equals $\tilde{v}^\star = Pe_{H,C}\, v^\star$ in the fluid domains, and 0 in the solid domain. Then (8) may write as

$$\tilde{v}^\star \partial_{z^\star} T^\star - \Delta_{\xi^\star} T^\star - \partial^2_{z^\star} T^\star = 0, \tag{A.1}$$

where we have denoted $\Delta_{\xi^\star} \equiv \partial^2_{x^\star} + \partial^2_{y^\star}$. This equation produces the following system

$$\frac{d}{dz}\phi(z) = A\,\phi(z) \tag{A.2}$$

with A defined as

$$A = \begin{pmatrix} \tilde{v}^\star & -\Delta_{\xi^\star} \\ 1 & 0 \end{pmatrix}, \text{ with } \quad \phi = \begin{pmatrix} \partial_{z^\star} T^\star \\ T^\star \end{pmatrix} \tag{A.3}$$

Then it is possible to show that this operator A associated with various lateral boundary conditions is self-adjoin and compact which ensures the existence of a unique spectral decomposition. It was also shown in previous papers [25,26,7] assuming either infinite, semi-infinite or finite dimension exchangers, that the dimensionless temperature field can be written in a general classical form

$$T^\star = \sum_{n \in \mathbb{Z}^\star} x_n T_n e^{\lambda_n Z} \tag{A.4}$$

with x_n the modes amplitudes, T_n the modes and λ_n the eigenvalues of operator A, so that they are the solutions of the following generalized eigenmode problem:

$$A\,\phi_n = \lambda_n \phi_n, \tag{A.5}$$

with $\phi_n = \begin{pmatrix} \lambda_n T_n \\ T_n \end{pmatrix}$ or equivalently T_n will be solution of the following non-linear eigen-problem

$$\lambda_n \tilde{v}^\star T_n - \Delta_{\xi^\star} T_n - \lambda_n^2 T_n = 0 \tag{A.6}$$

where, again, we have denoted $\Delta_{\xi^\star} \equiv \partial^2_{x^\star} + \partial^2_{y^\star}$ and with an associated boundary condition at the lateral exchanger external interface with air

$$\partial_n T_n = Bi(T_n - T_a^\star) \tag{A.7}$$

It is interesting to mention that this boundary condition provides a constraint on the spectrum, generally called a 'compatibility condition', which can be simply obtained from applying the divergence theorem to (A.6), so that, the following equality has to be fulfilled

$$\lambda_n \langle T_n \rangle_c - Bi\left(\int_{\mathcal{C}^E} T_n d\mathcal{C}^E - 2\pi R_E T_a^\star\right) - \lambda_n^2 \int_{\mathcal{C}^E} T_n d\xi^\star = 0, \tag{A.8}$$

where again $\langle T_n \rangle_c$ denotes the mixing-cup average. Hence, one can see from (A.8) which is a second order equation in λ_n that λ_n is a *non-linear* function of *Bi*.

A.2. Asymptotic behavior at Bi ≪ 1

Since, (A.8) for each mode is indeed quadratic in λ_n, one should seek for a regular asymptotic expansion in $\sqrt{Bi}$ in the small *Bi* limit,

$$\begin{aligned} T_n &= T_n^{(0)} + \sqrt{Bi} T_n^{(1)} + Bi T_n^{(2)} + Bi^{3/2} T_n^{(3)} + \cdots \\ \lambda_n &= \lambda_n^{(0)} + \sqrt{Bi} \lambda_n^{(1)} + Bi \lambda_n^{(2)} + Bi^{3/2} \lambda_n^{(3)} + \cdots \end{aligned} \tag{A.9}$$

Using (A.9) in (A.6), it is possible to find that the sequence is closed and provides a hierarchy of well-defined coupled iterative problems. Let us now analyze some properties of the first corrections. The leading order term in the sequence fulfills

$$\begin{aligned} &\lambda_n^{(0)} \tilde{v}^\star T_n^{(0)} - \Delta_{\xi^\star} T_n^{(0)} - \lambda_n^{(0)2} T_n^{(0)} = 0 \\ &\partial_n T_n^{(0)}|_{\mathcal{C}^E} = 0 \end{aligned} \tag{A.10}$$

Then, again, using the divergence theorem, one finds the compatibility condition for the leading order eigenvalue estimate $\lambda_n^{(0)}$,

$$\lambda_n^{(0)} \left(\langle T_n^{(0)} \rangle_c + \lambda_n^{(0)} \int_{C_E} T_n^{(0)} d\xi^\star \right) = 0, \tag{A.11}$$

where, again, $\langle T_n^{(0)} \rangle_c$ refers to the mixing-cup temperature. In the special case, $n = 0$, the solution of (A.10) is a constant $T_0^{(0)} = C_0^0$, leading to the simple mixing-cup $\langle T_0^{(0)} \rangle_c = C_0^0 Q^\star Pe$ which, in the case of a balanced configuration where $Q^\star = 0$, and since $C_0^0 \neq 0$, leads to $\lambda_0^{(0)} = 0$. Now considering the next term in the sequence, for a balanced configuration, one finds

$$\begin{aligned} &\Delta_{\xi^\star} T_n^{(1)} = \lambda_n^{(1)} \left(\tilde{v}^\star + 2\lambda_n^{(0)} \right) T_n^{(0)} \\ &\partial_n T_n^{(1)}|_{\mathcal{C}^E} = 0 \end{aligned} \tag{A.12}$$

The compatibility condition again obtained with the divergence theorem, provides

$$\lambda_n^{(1)} \left(\langle T_n^{(0)} \rangle_c + 2\lambda_n^{(0)} \int_{C_E} T_n^{(0)} d\xi^\star \right) = 0, \tag{A.13}$$

In the special case $n = 0$, for a balanced configuration, one immediately realizes that (A.13) is always true, since, $\langle T_0^{(0)} \rangle_c = Pe C_0^0 Q^\star = 0$ and $\lambda_0^{(0)} = 0$. Hence, (A.13) does not provide any constraint on $\lambda_0^{(1)}$ correction which is thus non-zero. Hence, $\lambda_0^{(1)}$ is the leading order term of sequence (A.9), thus justifying the numerical result provided in (25).

Appendix B. Numerical implementation

The details of the numerical implementation of the generalized Graetz problem can be found in [24]. This paper treats a very general case with multiple boundary conditions, we will only consider the case of continuous boundary conditions between inlet/outlet tubes and the exchanger. The conditions are referred to as coupling conditions.

$$\begin{aligned} &T^\star_{left} = T^\star_{right} \quad \text{on } D^{H,C}_{0,L} \\ &\partial_{z^\star} T^\star_{left} = \partial_{z^\star} T^\star_{right} \quad \text{on } D^{H,C}_{0,L} \end{aligned} \tag{B.1}$$

The main idea is to separate the whole problem into three separate Graetz problems: in inlet tubes, one in outlet tubes and one in the exchanger. Each Graetz problem follows a different expression of the dimensionless temperature field since there is a different spectral decomposition. It has been proven in [8], that there exists a general solution of the whole problem which satisfies the continuity conditions between the inlet/outlet tubes and the exchanger.

In order to provide those coupling conditions between inlet/outlet tubes and the exchanger, one defines a cost function as in [24]

$$J_{\mathcal{L}_2}(T^\star) = \int_{D^{H,C}_{0,L}} \left| T^\star_{left} - T^\star_{right} \right|^2 \mathrm{d}s + \in_{D^{H,C}_{0,L}} \left| \partial_z T^\star_{left} - \partial_z T^\star_{right} \right|^2 \mathrm{d}s \tag{B.2}$$

$T^\star$ is defined on a infinite dimension space of the general Graetz decomposition on the whole problem *V*. We define the different Graetz decompositions which correspond to different spaces on the inlet/outlet tubes and the exchanger as follow

$$V^0 = \left\{ T^\star(\xi^\star, z^\star) = \sum_{\mathbb{N}^*} x_n^+ T_n^+(\xi^\star) e^{\lambda_n^+ z^\star} + x_n^- T_n^-(\xi^\star) e^{\lambda_n^-(z^\star - L^\star)} \right\}$$
exchanger $z^\star \in [0, L^\star]$

$$V^1 = \{ T^\star(\xi^\star, z^\star) = x_0^H + \sum_{\mathbb{N}^*} x_n t_n^+(\xi^\star) e^{\mu_n^+(z^\star - L^\star)} \}$$
hot outlet tube $z^\star \geqslant L^\star$

$$V^2 = \left\{ TT^\star(\xi^\star, z^\star) = x_0^C + \sum_{\mathbb{N}^*} x_n t_n^-(\xi^\star) e^{\mu_n^- z^\star} \right\}$$
cold outlet tube $z^\star \leqslant 0$

$$V^3 = \left\{ T^\star(\xi^\star, z^\star) = T_H^{\star -\infty} + \sum_{\mathbb{N}^*} x_n t_n^-(\xi^\star) e^{\mu_n^- z^\star} \right\}$$
hot inlet tube $z^\star \leqslant 0$

$$V^4 = \left\{ T^\star(\xi^\star, z^\star) = T_C^{\star +\infty} + \sum_{\mathbb{N}^*} x_n t_n^+(\xi^\star) e^{\mu_n^+(z^\star - L^\star)} \right\}$$
cold inlet tube $z^\star \geqslant L^\star$

(B.3)

where $x_n^\pm$ are the generalized Graetz modes amplitudes, $T_n^\pm$ are the upstream and downstream exchanger Graetz modes, $t_n^\pm$ are the upstream and downstream Graetz modes in the inlet and outlet tubes, $\lambda_n^\pm$ are the upstream and downstream Graetz eigenvalues inside the exchanger and μ_n^+ are downstream Graetz eigenvalues in the hot outlet tube and cold inlet tube, μ_n^- are upstream Graetz eigenvalues in the cold outlet tube and hot inlet tube.

Let us note that the eigenvalues $\lambda_n^\pm$ verify by definition $\lambda_n^+ = \lambda_n$, $\lambda_n^- = \lambda_{-n}$ and

$$-\infty \underset{n\to+\infty}{\longleftarrow} \lambda_n \leqslant \cdots \leqslant \lambda_1 < 0 < \lambda_{-1} < \cdots \leqslant \lambda_{-n} \underset{n\to+\infty}{\longrightarrow} +\infty \tag{B.4}$$

V is then defined as $V = V^0 \cup V^0 \cup V^1 \cup V^2 \cup V^3 \cup V^4$. The numerical approximation consists of a projection of the space V on a space V_N of finite dimension N, which means that one only considers a finite number N of Graetz modes to compute the dimensionless temperature field $T^\star$.

Let $(e_k)_{k=1\ldots N}$ be a basis of the space V_N and let us write

$$J_{\mathcal{L}_2} = m(T^\star, T^\star) + b(T^\star) + c \tag{B.5}$$

where m is bi-linear symmetric, b linear and c a constant. Let $\mathbf{M}_{\mathcal{L}_2} \in \mathbb{R}^{N\times N}$ and $\mathbf{b} \in \mathbb{R}^N$ defined as $\mathbf{M}_{\mathcal{L}_2\,ij} = m(e_i, e_j)$ and $\mathbf{b}_i = b(e_i)$. Then, the minimization problem writes as: find $\mathbf{x} \in \mathbb{R}^N$ solution of,

$$\mathbf{M}_{\mathcal{L}_2}\mathbf{x} = \mathbf{b} \tag{B.6}$$

which is a simple linear system to inverse to get the amplitudes of the Graetz modes. The practical construction of the matrix $\mathbf{M}_{\mathcal{L}_2}$ can be found on [24]. It is important to stress that this matrix can be small, since the number of modes needed to construct a proper field $T^\star$ doesn't need to be large. Let us also emphasize the fact that this numerical method solves a 2D problem to compute the eigenvalues and eigenvectors and inverse a small matrix to guarantee coupling conditions. The 3D-reconstruction is done using the analytically decomposition (B.3) so the method is computationally efficient.

Appendix C. Numerical validation

We present in this section a numerical validation (see Tables C.1 and C.2) based on the anti-symmetry of eigenvalues in the exchanger in a counter-flow configuration, which means that $\lambda_{-i} = -\lambda_i$ i.e. $\lambda_i^+ = -\lambda_i^-$ for all $i \in I$, where I is the set that indexes the spectrum of the operator of the main problem. Indeed, the scalar values λ_i do not depend on the orientation of axes of coordinates $x^\star$, $y^\star$ and $z^\star$.

Let us also show an anti-symmetry of the Graetz modes $T_i(x^\star, y^\star) = -T_{-i}(-x^\star, y^\star)$. Using previous notations, one has

$$\begin{aligned} A\phi_i &= \lambda_i \tilde{v}^\star \phi_i \\ A\phi_{-i} &= \lambda_{-i} \tilde{v}^\star \phi_{-i} \end{aligned} \tag{C.1}$$

By applying an anti-symmetry operator S such as $S(T_i(x,y)) = T_i(-x,y)$ on the second equation, one gets

$$\begin{aligned} AS\phi_{-i} = \lambda_{-i} S\tilde{v}^\star S\phi_{-i} &= -\lambda_i(-\tilde{v}^\star(x^\star, y^\star))S\phi_{-i} \\ &= \lambda_i \tilde{v}^\star(x^\star, y^\star)S\phi_{-i} \end{aligned} \tag{C.2}$$

Table C.1
Relative errors of efficiencies $\epsilon_C - \epsilon_H$, first eigenvalue $\lambda_+^0 + \lambda_-^0$ and second eigenvalue $\lambda_+^1 + \lambda_-^1$ for various values of Pe, l, Bi and k^S.

Pe	L	Bi	k^S	$\lvert\epsilon_C - \epsilon_H\rvert$	$\lvert\lambda_+^0 + \lambda_-^0\rvert$	$\lvert\lambda_+^1 + \lambda_-^1\rvert$
15.0	10.0	0.001	1.0	1.393760e−07	2.027600e−10	2.021400e−08
			10.0	7.380780e−07	2.987000e−10	1.367290e−07
		1000.0	1.0	6.533600e−08	4.921000e−08	9.932100e−07
			10.0	2.469819e−06	2.445040e−07	2.560937e−03
	20.0	0.001	1.0	9.455200e−08	2.027600e−10	2.021400e−08
			10.0	4.338670e−07	2.987000e−10	1.367290e−07
		1000.0	1.0	9.594700e−08	4.921000e−08	9.932100e−07
			10.0	2.418371e−06	2.445040e−07	2.560937e−03
100.0	10.0	0.001	1.0	9.061540e−07	4.070000e−11	2.957130e−07
			10.0	1.576944e−06	9.161000e−11	1.457733e−06
		1000.0	1.0	5.302000e−07	8.492800e−09	4.174500e−07
			10.0	8.544400e−07	3.983690e−08	1.012964e−04
	20.0	0.001	1.0	8.852740e−07	4.070000e−11	2.957130e−07
			10.0	1.251659e−06	9.161000e−11	1.457733e−06
		1000.0	1.0	4.203330e−07	8.492800e−09	4.174500e−07
			10.0	4.641510e−07	3.983690e−08	1.012964e−04

Table C.2
Values of eigenvalues λ_+^0, λ_+^1, λ_+^2, λ_+^3 for various values of Pe, l, Bi and k^S.

Pe	L	Bi	k^S	λ_+^0	λ_+^1	λ_+^2	λ_+^3
15.0	10.0	0.001	1.0	8.170724e−03	4.398618e−01	4.566489e−01	5.910715e−01
			10.0	1.253764e−02	7.244966e−01	1.016178e+00	1.085381e+00
		1000.0	1.0	1.549455e−01	7.018758e−01	7.319594e−01	9.940608e−01
			10.0	3.911171e−01	1.152600e+00	1.155169e+00	1.902514e+00
	20.0	0.001	1.0	8.170724e−03	4.398618e−01	4.566489e−01	5.910715e−01
			10.0	1.253764e−02	7.244966e−01	1.016178e+00	1.085381e+00
		1000.0	1.0	1.549455e−01	7.018758e−01	7.319594e−01	9.940608e−01
			10.0	3.911171e−01	1.152600e+00	1.155169e+00	1.902514e+00
100.0	10.0	0.001	1.0	1.314427e−03	1.182446e−01	1.226305e−01	2.606066e−01
			10.0	2.259361e−03	1.873122e−01	1.886942e−01	2.946533e−01
		1000.0	1.0	2.407891e−02	1.284228e−01	1.309758e−01	2.927729e−01
			10.0	6.087998e−02	1.944533e−01	1.945562e−01	3.946634e−01
	20.0	0.001	1.0	1.314427e−03	1.182446e−01	1.226305e−01	2.606066e−01
			10.0	2.259361e−03	1.873122e−01	1.886942e−01	2.946533e−01
		1000.0	1.0	2.407891e−02	1.284228e−01	1.309758e−01	2.927729e−01
			10.0	6.087998e−02	1.944533e−01	1.945562e−01	3.946634e−01

because of the anti-symmetry of v on x and $\lambda_i = -\lambda_{-i}$. Then, by using both equations

$$A(\phi_i - S\phi_{-i}) = \lambda_i \tilde{v}^{\star}(\phi_i - S\phi_{-i}) \tag{C.3}$$

so that $\phi_i - S\phi_{-i}$ is a solution of the eigenvalue problem. Thus, one has

$$\phi_{-i} - S\phi_{-i} = \alpha\phi_{-i} \quad \text{with } \alpha \in \mathbb{R} \tag{C.4}$$

So that $(1-\alpha)\phi_i = S\phi_{-i}$ Since modes are normalized, $\|\phi_i\| = \|\phi_{-i}\| = \|S\phi_{-i}\|$, which gives $\alpha = 2$. Using (C.4), one has the stated result:

$$T_i(x^{\star}, y^{\star}) = -T_{-i}(-x^{\star}, y^{\star}) \tag{C.5}$$

Under the condition $T_H^{-\infty} = -T_C^{\infty}$, this leads to the fact that the dimensionless temperature field of the full exchanger problem verifies $T(x,y,z) = -T(-x,y,-z)$.

References

[1] J.C. Bradley, Counterflow, crossflow and cocurrent flow heat transfer in heat exchangers: analytical solution based on transfer units, Heat Mass Transfer 46 (4) (2010) 381–394.
[2] Y.P. Cheng, Z.G. Qu, W.Q. Tao, Y.L. He, Numerical design of efficient slotted fin surface based on the field synergy principle, Numer. Heat Transfer, Part A 45 (6) (2004) 517–538.
[3] R.C. Chu, R.E. Simons, M.J. Ellsworth, R.R. Schmidt, V. Cozzolino, Review of cooling technologies for computer products, IEEE Trans. Device Mater. Rel. 4 (4) (2004) 568–585.
[4] O.I. Craciunescu, T.V. Samulski, J.R. MacFall, S.T. Clegg, Perturbations in hyperthermia temperature distributions associated with counter-current flow: numerical simulations and empirical verification, IEEE Trans. Biomed. Eng. 47 (4) (2000) 435–443.
[5] W. Escher, B. Michel, D. Poulikakos, Efficiency of optimized bifurcating tree-like and parallel microchannel networks in the cooling of electronics, Int. J. Heat Mass Transfer 52 (5-6) (2009) 1421–1430.
[6] W. Escher, B. Michel, D. Poulikakos, A novel high performance, ultra thin heat sink for electronics, Int. J. Heat Fluid Flow 31 (4) (2010) 586–598.
[7] J. Fehrenbach, F. De Gournay, C. Pierre, F. Plouraboué, The generalized Graetz problem in finite domains, SIAM J. Appl. Math. 72 (2012) 99–123.
[8] J. Fehrenbach, F. De Gournay, F. Plouraboué, Shape optimization for the generalized Graetz problem, Struct. Multidiscip. Optim. 49 (2014) 993–1008.
[9] A. Filali, L. Khezzar, Numerical simulation of the Graetz problem in ducts with viscoelastic FENE-P fluids, Comput. Fluids 84 (2013) 1–15.
[10] H.W. Huang, W.L. Lin, E.G. Moros, A robust power deposition scheme for tumors with large counter-current blood vessels during hyperthermia treatment, Appl. Therm. Eng. 89 (2015) 897–907.
[11] H. Kobayashi, S. Lorente, R. Anderson, A. Bejan, Serpentine thermal coupling between a stream and a conducting body, J. Appl. Phys. 111 (19–20) (2012) 044911.
[12] G. Maranzana, I. Perry, D. Maillet, Mini- and micro-channels: influence of axial conduction in the walls, Int. J. Heat Mass Transfer 47 (17–18) (2004) 3993–4004.
[13] I.C. Mihai, Heat transfer in minichannels and microchannels CPU cooling systems, in: P. Schiopu, C. Panait, G. Caruntu, et al. (Eds.), Advanced Topics in Optoelectronics Microelectronics, and Nanotechnologies IV, Proceedings of SPIE-The International Society for Optical Engineering, vol. 7297, SPIE-The International Society for Optical Engineering, 2009.
[14] J.W. Mitchell, G.E. Myers, An analytical model of the counter-current heat exchange phenomena, Biophys. J. 8 (1968) 897–911.
[15] S. Mori, M. Kataya, A. Tanimoto, Performance of counterflow, parallel plate heat exchangers under laminar flow conditions, Heat Transfer Eng. 2 (1) (1980) 28–38.
[16] A. Nakayama, F. Kuwahara, A general bioheat transfer model based on the theory of porous media, Int. J. Heat Mass Transfer 51 (11–12) (2008) 3190–3199.
[17] R. Nunge, E.W. Porta, W.N. Gill, Axial conduction in the fluid streams of multistream heat exchangers, Chem. Eng. Progr. Symp. 63 (1967) 80–91.
[18] R.J. Nunge, W.N. Gill, Analysis of heat or mass transfer in some countercurrent flows, Int. J. Heat Mass Transfer 8 (1965) 873–886.
[19] R.J. Nunge, W.N. Gill, An analytical study of laminar counter flow double-pipe heat exchangers, AIChE J. 12 (1966) 279–289.
[20] D.A. Pabst, S.A. Rommel, W.A. McLellan, T.M. Williams, T.K. Rowles, Thermoregulation of the intra-abdominal testes of the bottlenose dolphin (Tursiops truncatus) during exercise, J. Exp. Biol. 198 (1995) 221–226.
[21] E. Papoutsakis, D. Ramkrishna, H-C. Lim, The extended Graetz problem with Dirichlet wall boundary conditions, Appl. Sci. Res. 36 (1980) 13–34.
[22] E. Papoutsakis, D. Ramkrishna, H-C. Lim, Conjugated Graetz problems. Pt. 1: General formalism and a class of solid–fluid problems, Chem. Eng. Sci. 36 (8) (1981) 1381–1391.
[23] T.L. Perelman, On conjugated problems of heat transfer, Int. J. Heat Mass Transfer 3 (4) (1961) 293–303.
[24] C. Pierre, J. Bouyssier, F. de Gournay, F. Plouraboué, Numerical computation of 3D heat transfer in complex parallel heat exchangers using generalized Graetz modes, J. Comp. Phys 268 (2014) 84–105.
[25] C. Pierre, J. Bouyssier, F. Plouraboué, Mathematical analysis of parallel convective exchangers with general lateral boundary conditions using generalized Graetz modes, Math. Models Methods Appl. Sci. 24 (4) (2013) 627–667.
[26] C. Pierre, F. Plouraboué, Numerical analysis of a new mixed-formulation for eigenvalue convection–diffusion problems, SIAM J. Appl. Math. 70 (2009) 658–676.
[27] F. Plouraboué, C. Pierre, Stationary convection–diffusion between two co-axial cylinders, Int. J. Heat Mass Transfer 50 (2007) 4901–4907.
[28] A.E. Quintero, M. Vera, B. Rivero-de Aguilar, Wall conduction effects in laminar counterflow parallel-plate heat exchangers, Int. J. Heat Mass Transfer 70 (1-3) (2014) 939–953.
[29] Ilya I. Ryzhkov, The extended Graetz problem with specified heat flux for multicomponent fluids with Soret and Dufour effects, Int. J. Heat Mass Transfer 66 (2013) 461–471.
[30] R.K. Shah, Dušan P. Sekulić, Fundamentals of Heat Exchanger Design, John Wiley and Sons, New Jersey, 2003.
[31] D. Shrivastava, B. McKay, R.B. Roemer, An analytical study of heat transfer in finite tissue with two blood vessels and uniform Dirichlet boundary conditions, ASME J. Heat Transfer 127 (2) (2005) 179–188.
[32] D. Shrivastava, R. Roemer, An analytical study of heat transfer in a finite tissue region with two blood vessels and general Dirichlet boundary conditions, Int. J. Heat Mass Transfer 48 (19–20) (2005) 4090–4102.
[33] S.N. Singh, Heat transfer by laminar flow in a cylindrical tube, Appl. Sci. Res. A7 (1958) 325–340.
[34] W.Q. Tao, Z.-Y. Guo, B.X. Wang, Field synergy principle for enhancing convective heat transfer: its extension and numerical verifications, Int. J. Heat Mass Transfer 45 (18) (2002) 3849–3856.
[35] M. Vera, A. Liñán, Laminar counter flow parallel-plate heat exchangers: exact and approximate solutions, Int. J. Heat Mass Transfer 53 (2010) 4885–4898.
[36] M. Vera, A. Liñán, Exact solution for the conjugate fluid–fluid problem in the thermal entrance region of laminar counterflow heat exchangers, Int. J. Heat Mass Transfer 54 (1–3) (2011) 490–499.
[37] W. Qu, I. Mudawar, Experimental and numerical study of pressure drop and heat transfer in a single-phase micro-channel heat sink, Int. J. Heat Mass Transfer 45 (2002) 2549–2565.
[38] B. Weigand, An extract analytical solution for the extended turbulent Graetz problem with Dirichlet wall boundary conditions for pipe and channel flows, Int. J. Heat Mass Transfer 39 (8) (1996) 1625–1637.
[39] B. Weigand, M. Kanzamar, H. Beer, The extended Graetz problem with piecewise constant wall heat flux for pipe and channel flows, Int. J. Heat Mass Transfer 44 (20) (2003) 3941–3952.
[40] B. Weigand, D. Lauffer, The extended Graetz problem with piecewise constant wall heat flux for laminar and turbulent flows inside concentric annuli, Heat Mass Transfer 39 (4) (2003) 313–320.
[41] B. Weigand, D. Lauffer, The extended Graetz problem with piecewise constant wall temperature for pipe and channel flows, Int. J. Heat Mass Transfer 24 (2004) 5303–5312.
[42] P. Yuan, Numerical analysis of an equivalent heat transfer coefficient in a porous model for simulating a biological tissue in a hyperthermia therapy, Int. J. Heat Mass Transfer 52 (7–8) (2009) 1734–1740.
[43] H. Zhang, A. Lorente, S. Bejan, Vascularization with line-to-line trees in counterflow heat exchange, Int. J. Heat Mass Transfer 52 (19–20) (2009) 4327–4342.
[44] Y. Zhang, Generalized dual-phase lag bioheat equations based on nonequilibrium heat transfer in living biological tissues, Int. J. Heat Mass Transfer 52 (21–22) (2009) 4829–4834.
[45] L. Zhu, Theoretical evaluation of contributions of heat conduction and counter-current heat exchange in selective brain cooling in humans, Ann. Biomed. Eng. 28 (2000) 269–277.